

1 **Supplementary Information to:**

2 **A comprehensive molecular profiling approach reveals metabolic**

3 **alterations that steer bone tissue regeneration**

4 Julia Löffler^{1,2,3}, Anne Noon^{1,2}, Agnes Ellinghaus^{1,2}, Anke Dienelt^{1,2}, Stefan Kempa³†* and Georg N.
5 Duda^{1,2}† *

6 ¹ Julius Wolff Institute (JWI), Berlin Institute of Health at Charité – Universitätsmedizin Berlin, 13353
7 Berlin, Germany

8 ² BIH Center for Regenerative Therapies (BCRT), Berlin Institute of Health at Charité –
9 Universitätsmedizin Berlin, 13353 Berlin, Germany

10 ³ Berlin Institute for Medical Systems Biology, Max-Delbrück-Center for Molecular Medicine, 10115,
11 Berlin, Germany

12 † These authors contributed equally to this work as senior author

13 **Running title: Metabolic alterations steer bone regeneration**

14 *Correspondence:

15 Prof. Dr.-Ing. Georg N. Duda, Julius Wolff Institute and Berlin Institute of Health Center for
16 Regenerative Therapies at Berlin Institute of Health and Charité – Universitätsmedizin Berlin,
17 Augustenburger Platz 1, D-13353 Berlin, Germany, e-mail: georg.duda@charite.de, telephone: +49 30
18 450559079, fax: +49 30 450 559969

19

20

21

22

23 **Supplement Methods**

24 **Experimental design – animal model**

25 Surgeries were performed on two groups: (1) 3 month old female Sprague-Dawley rats and (2)
26 12 months old female ex-breeder Sprague-Dawley rats that have had a minimum of three litters
27 (weight 400 ± 60 g), purchased at Charles River. Aged animals were purchased aged 7-8 months,
28 with the last litter was born approximately 4-6 weeks before delivery to our animal housing.
29 Since the companies do not keep the animals after exclusion from breeding, animals were kept
30 for 4-5 months in our in-house facilities before surgical procedure. Previously published studies
31 by Preininger et al., Strube et al. and Löffler et al. confirm these animals as a model for
32 biologically compromised fracture healing, resulting in the formation of a non-union without
33 further treatment during the investigation period ¹⁻⁵.

34 Animals received a 2mm osteotomy at the left femur under general anesthesia of 0.3 mg/kg
35 Medetomidin DomitorH and 60 mg/kg Ketamin administered i.p.. Additionally, 45 mg/kg
36 Clindamycin was administered by s.i. and eyes were prevented from drying out by application
37 of eye balm. For analgesia prior to the surgery the animals received 20 mg/kg Tramadol. A
38 longitudinal skin incision was made over the left femur and the bone exposed by blunt fascia
39 dissections. An in-house developed unilateral external fixator was mounted to stabilize the
40 bone, made of stainless steel and titanium as published previously. ³ To ensure the highest
41 possible standardization for placement of the four wire holes, a drilling template was used for
42 every surgery. After incision of the titanium wires, the external fixator bar was placed on the
43 wires and a standardized 2mm gap was sawn into the femoral bone. To ensure gap size
44 reproducibility a sawing template was used at all times. Muscle fascia and skin were closed
45 using absorbable and non-absorbable sutures, respectively. Tramadol as post-surgery analgesia
46 was administered for three days through the drinking water (25 ml/l). Animals were checked

47 daily for overall health status and fixator positioning. Bone healing was monitored over a period
48 of 2 weeks. Animals were sacrificed and femurs were sampled for histological assessment, gene
49 expression, protein, and metabolite levels at day 3, 7 and 14 after osteotomy. Animals were
50 assigned to the different groups randomly.

51 For samples not only the fracture tissue but also adjacent tissue, located 1 mm distal and
52 proximal to the fracture hematoma was samples. This was done aiming to include cells and
53 signals from the bone marrow that are attracted to the fracture site. This is especially relevant
54 in later time points of the healing cascade, where relevant players migrate from the bone marrow
55 cavity into the fracture gaps. In order to obtain tissue samples that can be compared in the best
56 possible/standardized way this approach was chosen.

57

58

59

60

61

62

63

64

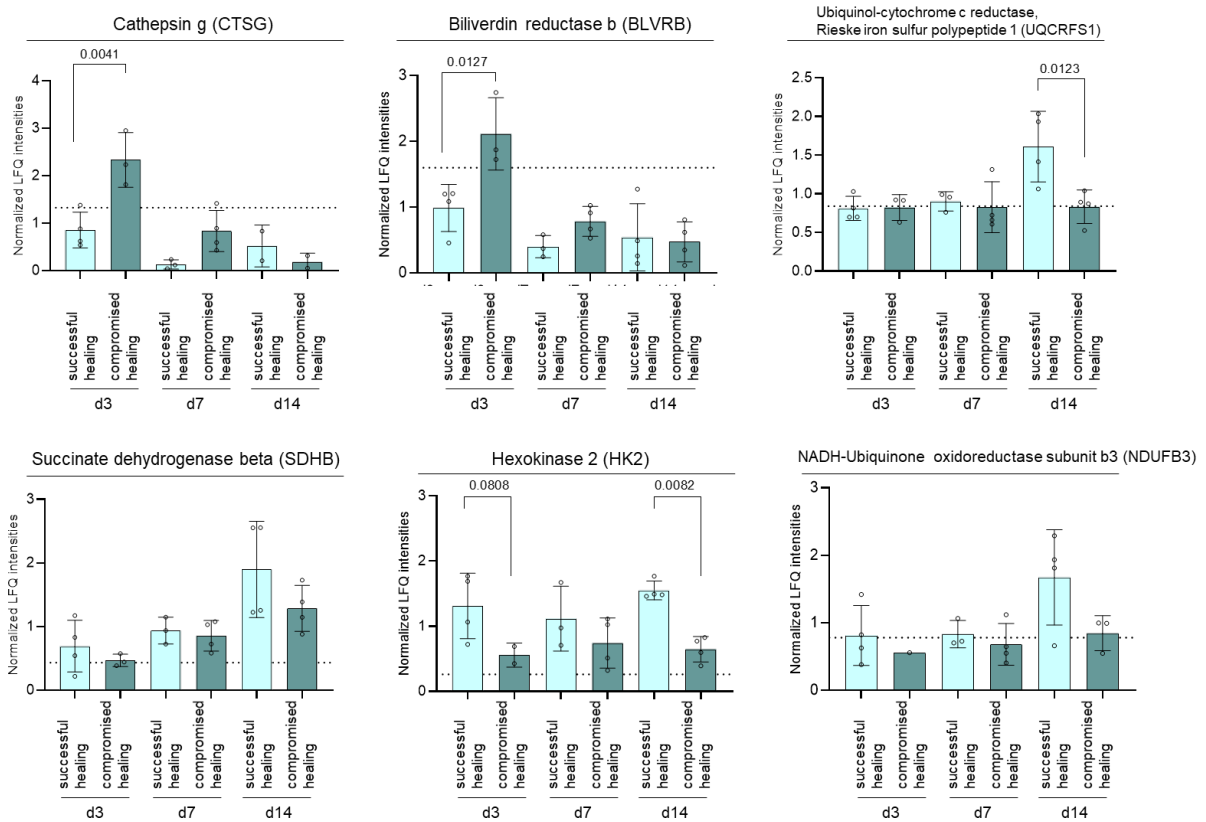
65

66

67

68

69 **Supplementary Figures**

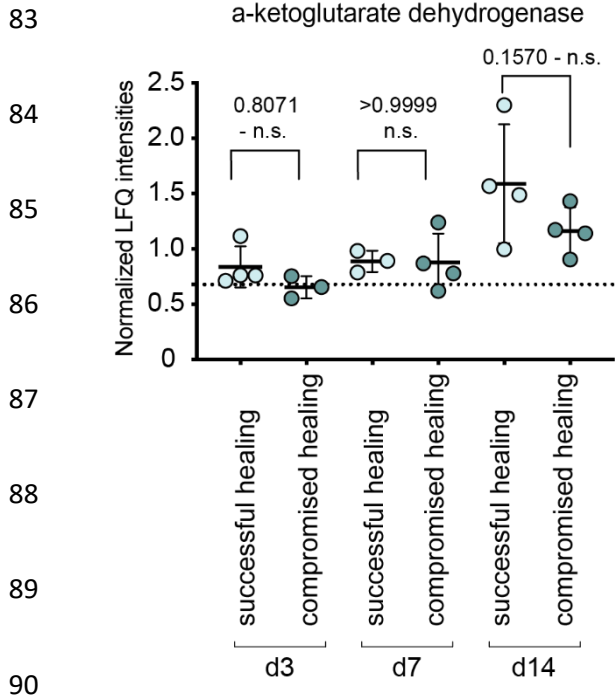


70

71 **Supplementary figure 1. Exemplary proteins and their abundance for the identified and**
 72 **regulated protein cluster in successful vs. compromised healing.** Cathepsin G and biliverdin
 73 reductase are representative for higher abundance of pro-inflammatory proteins in
 74 compromised healing, while ubiquinol-cytochrome c reductase, Rieske iron sulfur polypeptide
 75 1 and NADH-ubiquinone oxidoreductase subunit 3 show exemplary levels for oxidative
 76 metabolism. Succinate dehydrogenase beta and hexokinase 2 levels are representative higher
 77 for central carbon metabolism protein abundance in successful healing samples. The dotted line
 78 represents respective protein abundance in unfractured, contralateral femoral bone. Shown are
 79 mean±standard deviation, normalized label-free-quantification (LFQ) intensities, n=3-5
 80 individual biological replicates per group and time point, One-way ANOVA.

81

82

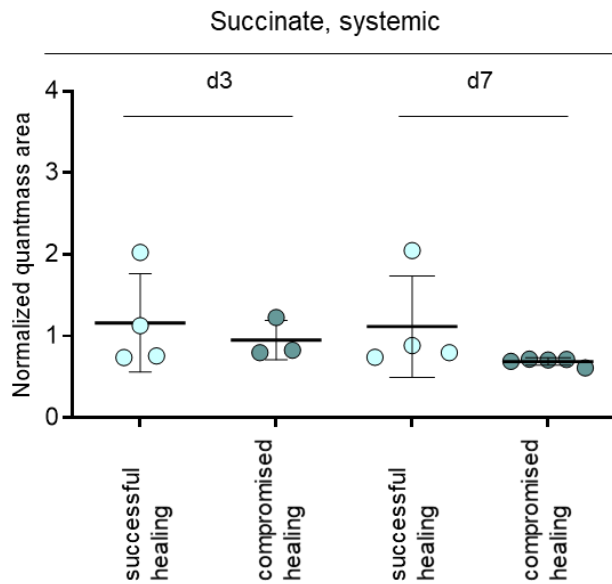


91 **Supplementary figure 2. OGDH protein levels between successful and compromised**
 92 **healing.** OGDH protein levels showed an increase at d14 after osteotomy in both healing groups
 93 (successful and compromised). The dotted line represents OGDH levels in unfractured,
 94 contralateral femoral bone. Shown are mean±standard deviation, normalized label-free-
 95 quantification (LFQ) intensities, n=3-5 individual biological replicate, per group and time point,
 96 One-way ANOVA.

97

98

99



100

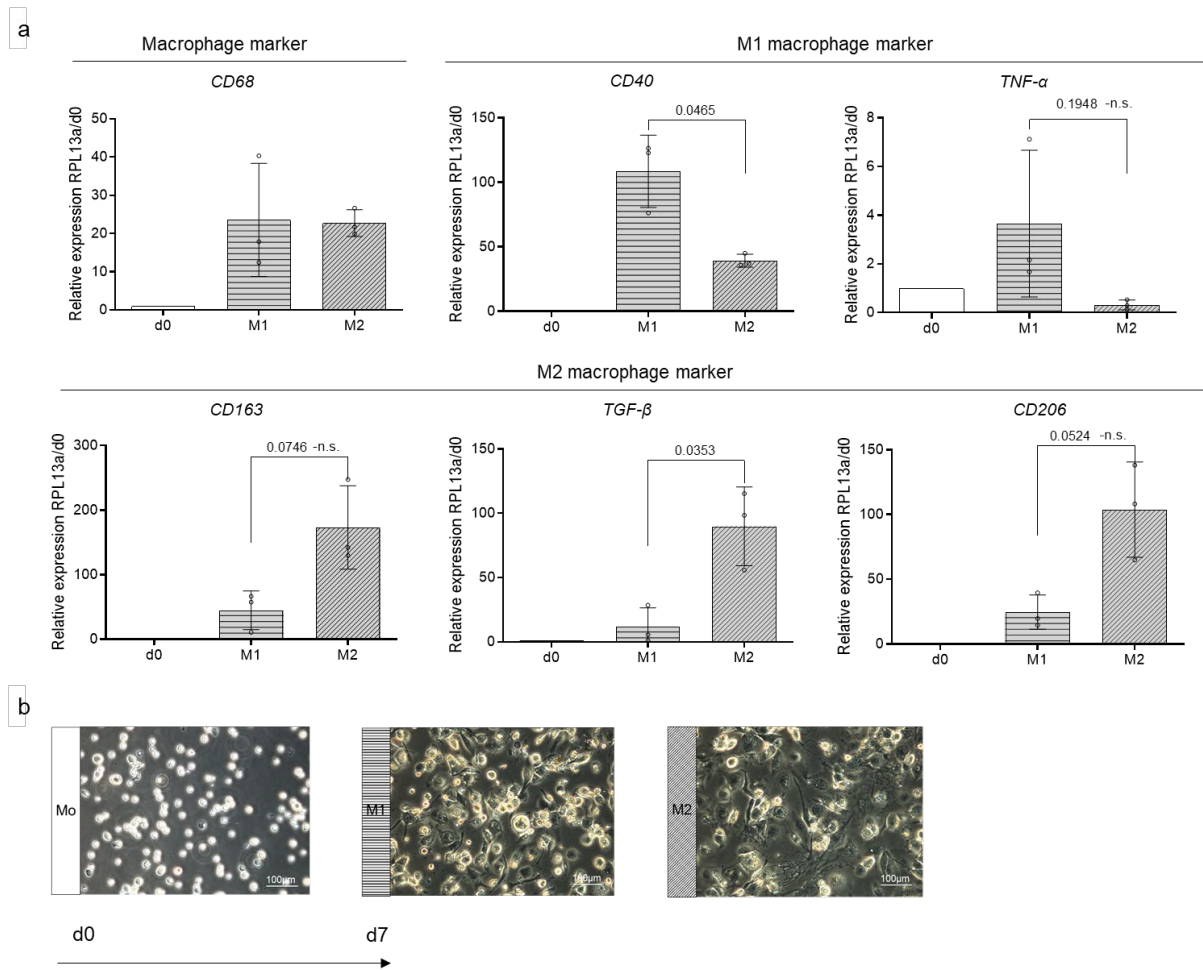
101 **Supplementary figure 3. Systemic levels of succinate show now alterations between**
 102 **healing time points or groups.**

103 Analysis of systemic succinate levels, from intracardiac blood collection showed no significant
 104 difference between compromised and successful healing at fracture healing onset (day 3, day
 105 7) nor significant level alterations between day 3 and day 7 within healing groups.

106 Mean±standard deviation, n=3-5 individual biological replicates per group and time point, t-
 107 test.

108

109



110

111 **Supplementary figure 4. THP-1 human monocytic cell line differentiation into M1 and**

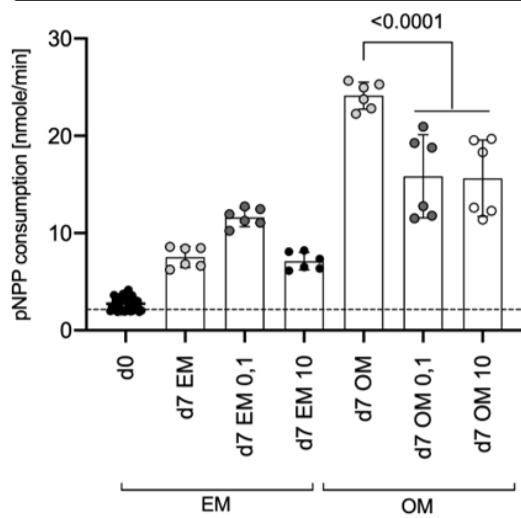
112 **M2 macrophages.** (a) The general marker for macrophages *CD68* is upregulated upon
 113 differentiation from monocytes to macrophages in both M1 and M2 polarized macrophages.

114 *CD40* and *TNF- α* marker for M1 macrophage polarization are upregulated in M1 polarized
 115 macrophages, while *TGF- β* and *CD206* – markers for the M2 subtype are upregulated in M2
 116 polarized macrophage cultures. Relative expression to RLP13a (housekeeping gene and day 0).

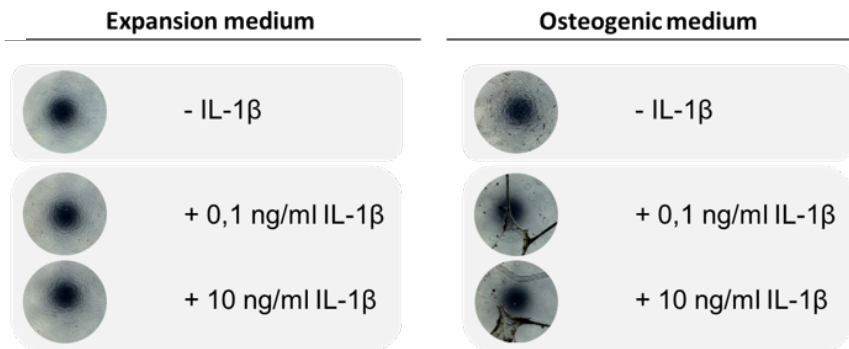
117 3-4 individual experimental replicates, mean \pm standard deviation, One-way ANOVA. (b)

118 Microscopic images of THP-1 monocytes (suspension cells) before differentiation (20x
 119 magnification). Microscopic images after 7 days of differentiation and polarization, M1
 120 polarized cultures (+LPS, +INF γ) and M2 polarized cultures (+IL-4, +IL-13) (20x
 121 magnification).

a Alkaline phosphatase activity – continuous IL-1 β



b



122

123 **Supplementary figure 5. Constant exposure of IL-1 β strongly diminished the osteogenic**

124 **differentiation capacity of primary human MSCs in vitro.** (a) Addition of 0.1ng/ml and

125 10ng/ml IL-1 β to osteogenic cultures, did not enhance osteogenic differentiation, as the early

126 marker for osteogenic differentiation, alkaline phosphatase activity, was significantly reduced

127 after 7 days of culture, pNPP - 4-nitrophenylphosphate. 6 individual experimental replicates,

128 mean \pm standard deviation, One-way ANOVA. (b) The cells in osteogenic conditions showed a

129 strong contraction and loss of cell layer integrity when IL-1 β was added to the culture, making

130 further analysis impossible, as shown in the microscopic images.

131

132

133

134

135

136

137

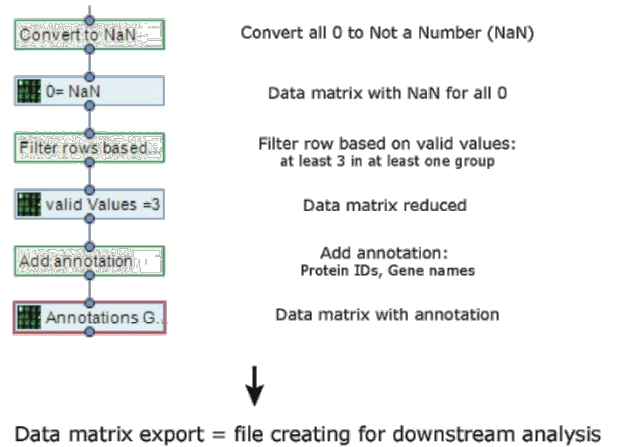
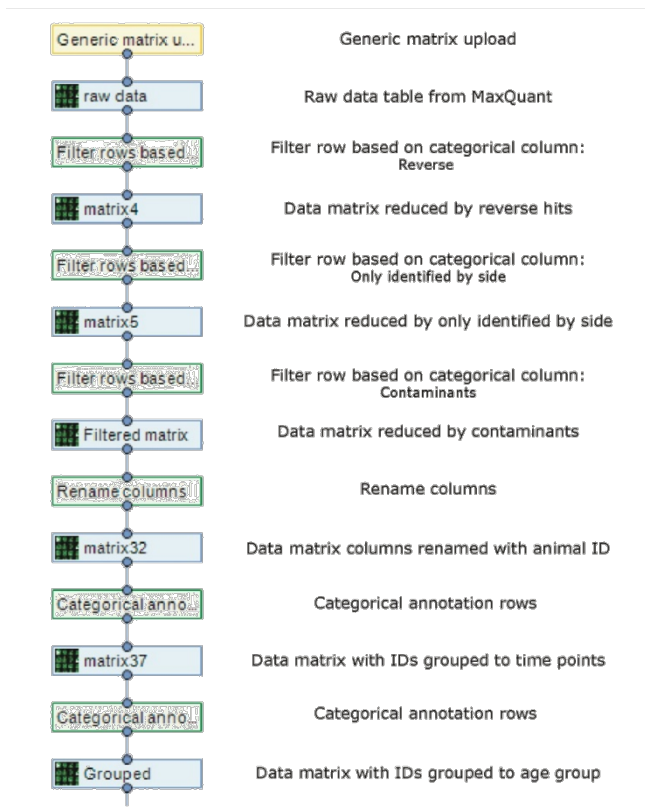
138

139

140

141

142



143

Supplementary figure 6. Schematic workflow of the processing of the data matrix from

144

MaxQuant using the Perseus software. Data matrix from MaxQuant is uploaded into Perseus,

145

contaminants and cleavage errors were excluded. Numerical IDs were replaced with animal

146

IDs, respective time point and grouped accordingly. All data points were no peptides were

147

measured (0) were replaced to NaN and matrix was filtered and reduced to proteins identified

148

at least 3 times per group (age). By upload of the uniprot data base: rattus norvegicus protein IDs

149

and gene names were added to the data. The data matrix was then exported for further analysis.

150

151

152

153

154 **Supplementary Tables**

155 **Supplementary Table 1. Animal treatment during surgical procedure.**

Substance	Concentration	Mode administered	Aim	Time point	Distributor
Medetomidin DomitorH	0.3mg/kg	Intraperitoneal injection	Anesthetic	Before surgery	OrionPharma, Germany
Ketamin	60mg/kg	Intraperitoneal injection	Anesthetic	Before surgery	Actavis, Ireland
Tramadol	20mg/kg	Intraperitoneal injection	Analgesia	Before surgery	Grünenthal, Germany
Clindamycin	45mg/kg	Subcutaneous injection	Antibiotic	Before surgery	Ratiopharm, Germany
Bepanthen® eye balm	-	Applied on eyes	Prevention of corneal drying out	Before surgery	Bayer Vital GmbH, Germany
Antisedan	1.5 mg/kg	Intraperitoneal injection	Anti-anesthetic	Post-surgery	Pfizer, Germany
Tramadol	25ml/l	Drinking water	Analgesia	3 days post-surgery	Grünenthal, Germany

156

157

158

159

160

161

162

163

164

165

166

167

168

169

170 **Supplementary Table 2. Primer pairs and sequences.**

Species	Gene	Gene Name	Forward 5'-3'	Reverse 5'-3'
human	<i>CD40</i>	Cluster of differentiation 40	ggttcacctcgctatggt	cagtgggtggttctggatg
	<i>CD68</i>	Cluster of differentiation 68	gtccacctcgacctgctct	cactggggcaggacaaaact
	<i>CD163</i>	Cluster of differentiation 163	tcagctgatttcagtgtgct	aggctgaactcactgggtataaat
	<i>CD206</i>	Cluster of differentiation 206	gggccaagcttctctggaat	tttatccacagccacgtccc
	<i>TNF-α</i>	Tumor necrosis factor alpha	tccccaggacctctcteta	gagggtttgctacaacatggg
	<i>TGF-β</i>	Transforming growth factor beta	gcgtgctaattggtggaaacc	gcttctcggagctctgatgt
	<i>IL-1β</i>	Interleukin -1 beta	gcgtgctaattggtggaaacc	gcttctcggagctctgatgt
	<i>RPL13A</i>	Ribosomal Protein 13a	cctggaggagaagaggaaagaga	ttgaggacctctgtgtatttgtcaa
rat	<i>Colla2</i>	Collagen type I alpha chain 2	ggagagagtgccaaactccag	ccaccccagggataaaaact
	<i>Spp1</i>	Osteopontin	gaggagaaggcgcattacag	atggctttcattggagttgc
	<i>Tbp</i>	Tata-box binding protein	ggaccagaacaacagccttc	ccgtaaggcatcattggact

171

172

173 **Supplementary References**

- 174 1 Preininger, B. *et al.* An Experimental Setup to Evaluate Innovative Therapy Options for the
175 Enhancement of Bone Healing Using Bmp as a Benchmark - a Pilot Study. *Eur Cells Mater* **23**,
176 262-272, doi:Doi 10.22203/Ecm.V023a20 (2012).
177 2 Strube, P. *et al.* Sex-specific compromised bone healing in female rats might be associated with
178 a decrease in mesenchymal stem cell quantity. *Bone* **45**, 1065-1072,
179 doi:<https://doi.org/10.1016/j.bone.2009.08.005> (2009).
180 3 Strube, P. *et al.* A new device to control mechanical environment in bone defect healing in rats.
181 *J Biomech* **41**, 2696-2702, doi:10.1016/j.jbiomech.2008.06.009 (2008).
182 4 Löffler, J. *et al.* Compromised Bone Healing in Aged Rats Is Associated With Impaired M2
183 Macrophage Function. *Frontiers in Immunology* **10**, doi:10.3389/fimmu.2019.02443 (2019).
184 5 Mehta, M., Duda, G. N., Perka, C. & Strube, P. Influence of gender and fixation stability on
185 bone defect healing in middle-aged rats: a pilot study. *Clinical orthopaedics and related*
186 *research* **469**, 3102-3110, doi:10.1007/s11999-011-1914-y (2011).

187